Published in final edited form as:
Neuron. 2008 March 27; 57(6): 917–929. doi:10.1016/j.neuron.2008.01.034.

Ivy Cells: A Population of Nitric-Oxide-Producing, Slow-Spiking GABAergic Neurons and Their Involvement in Hippocampal Network Activity

Pablo Fuentealba[1], **Rahima Begum**[2], **Marco Capogna**[1], **Shozo Jinno**[1,3], **László F. Márton**[1,4], **Jozsef Csicsvari**[1], **Alex Thomson**[2], **Peter Somogyi**[1], and **Thomas Klausberger**[1,5,*]

[1]MRC Anatomical Neuropharmacology Unit, Oxford University, Oxford OX1 3TH, UK

[2]Department of Pharmacology, The School of Pharmacy, University of London, 29-39 Brunswick Square, London WC1N 1AX, UK

[3]Department of Anatomy and Neurobiology, Graduate School of Medical Sciences, Kyushu University, Maidashi 3-1-1, Higashi-ku, Fukuoka 812-8582, Japan

[4]Neural Systems Research Group, Faculty of Engineering, EMTE-Sapientia Hungarian University of Transylvania, RO-540485 Targu Mures, Romania

[5]Center for Brain Research, Medical University of Vienna, 1090 Vienna, Austria

SUMMARY

In the cerebral cortex, GABAergic interneurons are often regarded as fast-spiking cells. We have identified a type of slow-spiking interneuron that offers distinct contributions to network activity. “Ivy” cells, named after their dense and fine axons innervating mostly basal and oblique pyramidal cell dendrites, are more numerous than the parvalbumin-expressing basket, bistratified, or axo-axonic cells. Ivy cells express nitric oxide synthase, neuropeptide Y, and high levels of $GABA_A$ receptor α1 subunit; they discharge at a low frequency with wide spikes in vivo, yet are distinctively phase-locked to behaviorally relevant network rhythms including theta, gamma, and ripple oscillations. Paired recordings in vitro showed that Ivy cells receive depressing EPSPs from pyramidal cells, which in turn receive slowly rising and decaying inhibitory input from Ivy cells. In contrast to fast-spiking interneurons operating with millisecond precision, the highly abundant Ivy cells express presynaptically acting neuromodulators and regulate the excitability of pyramidal cell dendrites through slowly rising and decaying GABAergic inputs.

INTRODUCTION

The activity of cortical neurons is embedded in network oscillations, which constitute a function of ongoing network operations, that are associated with behavior and the state of vigilance (Steriade et al., 2001). In the hippocampus, theta oscillations (4–10 Hz) occur during exploration and rapid eye movement sleep (Vanderwolf, 1969), together with gamma

*Correspondence: thomas.klausberger@pharm.ox.ac.uk.

SUPPLEMENTAL DATA

The Supplemental Data for this article can be found online at http://www.neuron.org/cgi/content/full/57/6/917/DC1/.

Europe PMC Funders Author Manuscripts

oscillations (30–80 Hz) (Csicsvari et al., 2003), which also correlate with working memory, conceptual categorization, attention, and perception (Singer and Gray, 1995). Sharp wave-associated ripples (100–200 Hz) occur in the hippocampus during consummatory behaviors and slow-wave sleep, and structure temporally compressed replay of waking neuronal activity (Buzsaki et al., 1983; Foster and Wilson, 2006; O'Keefe and Nadel, 1978). The different network states also require differential global state-dependent modulation, which is mostly provided by subcortical aminergic, cholinergic, GABAergic, and thalamic inputs. However, local slow signals may also make a contribution to regulating networks states, as can be assumed from the expression of a large number of neuropeptides by cortical neurons (Freund and Buzsaki, 1996). Oscillations in pyramidal cells (Soltesz and Deschenes, 1993) are shaped by the differential contribution of specialized GABAergic interneuron classes (Csicsvari et al., 1999; Klausberger et al., 2003).

In the cerebral cortex, different classes of GABAergic cell target specific subcellular domains of pyramidal cells (Ali et al., 1998; Miles et al., 1996; Somogyi and Klausberger, 2005). For example, basket cells innervate somata and proximal dendrites, whereas axo-axonic cells exclusively target axon-initial segments, and hippocampal bistratified cells innervate basal and oblique pyramidal cell dendrites (Somogyi et al., 1998). Similarly, cortical neuronal diversity has been explored on the basis of firing patterns; fast-spiking cells are recognized as interneurons (Connors et al., 1982; Ranck, 1973; Schwartzkroin and Kunkel, 1985), whereas some pyramidal cells are identified by their adapting firing patterns in the cortex (McCormick et al., 1985) or high-frequency bursts in the hippocampus (Ranck, 1973). As a result, most studies using extracellular unit recordings in behaving animals (Csicsvari et al., 1999) define interneurons by their narrow spike width and exclude slow-spiking units (Nitz and McNaughton, 2004) (e.g., firing rate <5 Hz). Immunohistochemical studies and gene expression profiles have distinguished interneuron populations according to the expression of molecular markers such as parvalbumin (PV)-, somatostatin (SM)-, cholecystokinin (CCK)-, or calretinin (CR)-immunoreactivities (Kawaguchi and Kondo, 2002; Toledo-Rodriguez et al., 2004). The electrophysiological and neurochemical characteristics of some interneurons have been found to correlate. For example, PV-expressing interneurons in the hippocampal CA1 pyramidal cell layer (basket, bistratified, and axo-axonic cells) often display a fast-spiking pattern of firing (Somogyi and Klausberger, 2005). Many studies have concentrated on these cells throughout the cortex, but they may not represent the majority of GABAergic neurons, since large populations of interneurons expressing neuropeptide Y (NPY) (Allen et al., 1983) or the neuronal nitric oxide (NO) synthase isoform (nNOS) (Czeh et al., 2005; Jinno and Kosaka, 2002) have also been reported. NO and NPY are implicated in regulating excitability and synaptic plasticity (Arancio et al., 1996; Colmers et al., 1987), yet little is known about the neuronal identity of their sources.

In the present study we have tested the hypothesis that NPY- and nNOS-expressing cells make contributions to network activity that are different from those made by PV-expressing interneurons. Furthermore, we have identified these cells based on their axo-dendritic distributions, their firing patterns, and the properties of their synaptic inputs and outputs, and we have quantified their abundance in relation to PV-expressing cells.

RESULTS

Cells Coexpressing nNOS and NPY form a Large Interneuron Population in the Hippocampus

We tested the abundance of nNOS- or NPY-expressing cells relative to PV-positive interneurons in the rat hippocampal CA1 area using the optical disector method and confocal laser scanning microscopy (Figure 1). In a triple immunoreaction, cells co-expressing nNOS and NPY were the most abundant population (37%), larger than the population expressing only PV (basket and axo-axonic cells, 26%) or PV and NPY (including bistratified cells; 15%) (Figure 1B and Table S1 available online). All NPY and nNOS coexpressing cells were PV immunonegative. The somata of the majority of these cells were located in stratum pyramidale and adjacent stratum radiatum, consistent with previous reports on nNOS (Czeh et al., 2005; Jinno and Kosaka, 2002). Further quadruple immunolabeling (Figure S1, available online, and Table S2) showed that all NPY and nNOS coexpressing cells were strongly immunopositive for the α1 subunit of the $GABA_A$ receptor ($GABA_AR$-α1) along the plasma membrane (n = 382), but less than 5% of NPY and nNOS coexpressing cells were immunopositive for CR, calbindin (CB), or SM (cells evaluated: n = 123, 148, and 137, respectively), similar to previous results on nNOS distribution (Czeh et al., 2005; Jinno and Kosaka, 2002). In addition, the somata of 75% of NPY and nNOS coexpressing cells in stratum pyramidale (n = 134) were also strongly immunolabeled in their somata for α-actinin-2, a cytoskeletal protein involved in cell signaling (Figure S1 and Table S2). Qualitative visual inspection revealed large populations of interneurons coexpressing NPY, nNOS, and $GABA_AR$-α1 in other regions of the hippocampus (CA2 and CA3 areas, dentate gyrus), and in extra-hippocampal cortical regions (subiculum, somatosensory cortex, and entorhinal cortex). Overall, these results reveal the existence of a major and distinct population of nNOS-, NPY-, and $GABA_AR$-α1-expressing interneurons.

Distinctive Dendritic and Axonal Arborizations Define the Ivy Cell

To determine the spike timing and axo-dendritic identity of NPY and nNOS coexpressing cells, we recorded interneurons in stratum pyramidale of anaesthetized rats and labeled them by the juxtacellular method for histological analysis. Four nNOS-expressing cells (P2a, T98e, T134a, and T140b) were recorded with their somata located in stratum pyramidale (Figure 2A). The soma area measured in the largest cross-section ranged from 87 to 145 μm^2, with the long axis between 13 and 19 μm and the short axis between 8 and 15 μm; the somata emitted five or six primary dendrites. The smooth, radially oriented dendrites (total extent: medio-lateral, 0.21 ± 0.05 mm; rostro-caudal, 0.35 ± 0.06 mm) rarely reached the border of stratum lacunosum-moleculare. The main axons profusely branched close to their origin, providing uncommonly dense, thin branches with minuscule varicosities, and extended 0.75 ± 0.12 mm in the medio-lateral and 1.31 ± 0.11 mm in the rostro-caudal directions. This cell type is distinguished by the exceptionally dense and fine axonal arborization close to the soma in strata oriens, radiatum, or both, and due to the resemblance of the axonal pattern to the ivy plant, so abundant in the English countryside, this interneuron type was named the “Ivy” cell. The axons of Ivy cells innervated strata radiatum and oriens to varying degrees (Figure 3A).

Due to the overlap in layer preference of the axonal arborizations of Ivy cells and the previously reported PV-expressing bistratified cells (Buhl et al., 1994; Klausberger et al., 2004; Pawelzik et al., 2002), we compared their axons quantitatively. The two-dimensionally projected axonal length was measured for every cell in three 100 × 100 μm squares in stratum oriens and proximal and distal stratum radiatum in a 70-μm-thick section containing the soma (Figure 3A). The squares were centered radially in line with the soma. The total projected axonal length of Ivy cells in the measured areas (2140 ± 325 μm; n = 4) was significantly longer (p = 0.016) than that of bistratified cells (954 ± 68 μm; n = 5, cells reported previously) (Klausberger et al., 2004). Ivy cells concentrated their axons next to stratum pyramidale, and thus axonal length quickly decreased as a function of distance from the soma. Conversely, the axonal fields of bistratified cells were more homogeneous across stratum radiatum, and somewhat sparser in stratum oriens (Figure 3A). The projected axonal length of Ivy cells in stratum oriens was ten times greater than that of bistratified cells (Figure 3A), a finding which suggests a massive difference in axon density between the two cell types.

Random samples of axons from three Ivy cells were further evaluated by electron microscopy to identify their postsynaptic targets. In contrast to most interneuron axons, the thin axons of Ivy cells had rather insignificant boutons containing a modest number of vesicles and infrequent mitochondria. In addition, vesicles were frequently found in preterminal axons away from synaptic specializations. The areas of presynaptic boutons from Ivy cells (n = 9 for P2a; n = 13 for T134a; n = 10 for T140b) and bistratified cells (n = 9 for T79e; n = 9 for T92a; n = 10 for T96b) were measured with electron microscopy from one 70-nm-thick section containing the synaptic specialization. The bouton areas of Ivy cells ($100.6 \pm 53.4 \times 10^3$ nm^2) were significantly smaller ($p < 0.0001$) than those of bistratified cells ($198.5 \pm 93.2 \times 10^3$ nm^2).

The randomly sampled synapses (n = 11 for P2a; n = 13 for T134b; n = 10 for T140b) had small synaptic junctions targeting mainly dendritic shafts (81%, Figures 3E and 3H) of pyramidal cells, including basal dendrites in stratum oriens and oblique dendritic shafts in stratum radiatum. Both basal and oblique dendrites are also innervated by PV-expressing bistratified cells. The mean diameter of pyramidal cell dendrites postsynaptic to Ivy cells was 0.49 ± 0.25 μm (n = 28), and not significantly different (p = 0.052) from the targets of bistratified cells (0.58 ± 0.13 μm, n = 27). Dendritic spines (13%) and apical dendrites of pyramidal cells (6%) were less frequent postsynaptic targets. Interneurons were not found among the synaptic targets in the random sample, and the identity of two postsynaptic targets could not be unequivocally determined.

In addition to the random sample, we specifically tested potential postsynaptic targets of Ivy cell T134a in the pyramidal cell layer. Of the 20 axonal varicosities examined in serial electron microscopic sections, five could be shown to establish synaptic junctions, three with small dendritic shafts and two with somata of pyramidal cells. Because only a small fraction of the axon was within the pyramidal cell layer, somata comprise only a small proportion of the overall targets of this cell.

Molecular Expression Profiles of Identified Ivy Cells

The labeled Ivy cells were tested for the expression of various molecular cell markers involved in intercellular signaling using immunofluorescence microscopy (Table 1). All four Ivy cells were immunopositive for nNOS in their somata (Figure 2C), proximal dendrites, or axons (Figures 3C and 3D). Three tested Ivy cells were immunopositive for NPY (soma), $GABA_AR$-α1 (somato-dendritic plasma membrane), and GAD (axon), confirming their identity as GABAergic interneurons (Figure 2C, Figure S2, and Table 1). None of the four cells expressed PV or SM, differentiating them from bistratified cells (Klausberger et al., 2004; Pawelzik et al., 2002). Furthermore, the tested cells were immunonegative for CCK, CB, vasoactive intestinal polypeptide (VIP), CR, muscarinic acetylcholine receptor 2, metabotropic glutamate receptor 1α (mGlur1α), α-actinin-2 (one cell tested), μ-opioid receptor, preprotachykinin A or B, the Kv3.1b subunit of K^+ channel, and metabotropic glutamate receptor 8a (mGlur8a) in their input terminals (Table 1).

Firing Patterns of Ivy Cells during Network Oscillations in Anaesthetized Rats

The firing of four identified Ivy cells was recorded during theta oscillations (4.2 ± 0.1 Hz), gamma oscillations (39.6 ± 1.5 Hz), and sharp wave-associated ripples (118 ± 5.7 Hz). The four Ivy cells discharged at similar frequencies ($p = 0.276$, Kruskal-Wallis test) during theta oscillations, non-theta/non-sharp wave periods, and sharp wave-associated ripples (0.7 ± 0.7, 1.7 ± 0.3, and 0.8 ± 1.1 Hz, respectively; Table S3), but discharge rates of single cells varied considerably within the same brain state (Figure S3).

Although discharge frequencies were low, Ivy cells showed clear phase preferences during hippocampal rhythms. They fired after the trough (30.7° ± 63.1°, mean angle ± angular deviation; 0° and 360° mark the trough) of the theta cycles recorded extracellularly in stratum pyramidale (Figure 4A, Table S3), just after the maximum discharge probability of pyramidal cells (Csicsvari et al., 1999; Klausberger et al., 2003). Phase preference, discharge frequency, and probability were all significantly different from those of bistratified cells (Figure S3). Like pyramidal cells (Csicsvari et al., 2003), recorded Ivy cells fired in a sparse (0.7 ± 0.6 Hz) yet phase-modulated way (Rayleigh test, $p < 0.01$; $r = 0.29 \pm 0.07$), which correlated with the troughs of gamma oscillations (10.6° ± 68°, Figure 4B). When Ivy cell firing during ripple oscillations was compared with their firing during neighboring non-theta/non-sharp wave episodes, it did not differ significantly in rate (Figure 4C). However, Ivy cells remained silent during the large majority of ripple episodes (>90%, Figure S3).

The action potentials recorded from Ivy cells were unusually broad for interneurons; we compared them here with the spikes of eight fast-spiking bistratified cells also recorded in vivo and reported previously (Klausberger et al., 2004) (Figure 4D). Spike duration (baseline-to-baseline; $p = 0.003$; 1.82 ± 0.45 and 0.95 ± 0.19 ms, for Ivy and bistratified cells, respectively) and width at maximal amplitude (positive peak to negative peak; $p = 0.004$; 0.56 ± 0.12 and 0.28 ± 0.01 ms, for Ivy and bistratified cells, respectively) were significantly longer lasting in Ivy than in bistratified cells, although there was no difference in action potential amplitude (positive peak to negative peak; $p = 0.414$; 1.12 ± 0.18 and 1.66 ± 0.80 mV, for Ivy and bistratified cells, respectively). Further comparison established

that the main difference between spike waveforms was in the decaying phase (10%–90% slope; $p = 0.004$; −3.23 ± 1.18 and −8.02 ± 3.72 mV/ms, for Ivy and bistratified cells, respectively) and not in the rising phase (10%–90% slope; $p = 0.414$; 2.22 ± 0.71 and 2.91 ± 1.22 mV/ms, for Ivy and bistratified cells, respectively), a result that is consistent with the presence of more slowly repolarizing K^+ currents in Ivy cells. This difference might be due, at least partially, to the absence of the Kv3.1b subunit in these cells (Table 1), a subunit that is expressed by most PV-containing cortical interneurons, including bistratified cells, and which contributes to their characteristic fast-spiking pattern (Martina et al., 1998; Rudy and McBain, 2001). A relatively low discharge frequency (Table S3) and broad spike width (Figure 4D) identify Ivy cells as slow-spiking GABAergic interneurons.

Firing Patterns of Putative Ivy Cells in Behaving Rats

To test whether interneurons with firing patterns similar to those of Ivy cells can be recognized in the pyramidal cell layer of nonanaesthetized animals, neuronal spiking activity was recorded with tetrodes in behaving animals. Sixteen interneurons were selected according to their spike timing around the trough of theta waves and the absence of significant changes in firing during ripple episodes. Further analysis showed that 8 out of those 16 cells exhibited slow spikes with more than 0.25 ms half-width (see Experimental Procedures) (Figure 5). The lack of complex spike bursts, as indicated by the first moment of their autocorrelogram, confirmed the eight units to be putative interneurons rather than pyramidal cells, and therefore these eight interneurons resemble identified Ivy cells recorded in anaesthetized animals. Interestingly, the discharge frequencies of all eight cells were low and, on average, similar during different brain states (2.4 ± 1.8; 6.7 ± 9.7, and 3.0 ± 3.6 Hz during theta, ripple, and non-theta/non-sharp episodes, respectively; $p = 0.543$, Kruskal-Wallis test; Figure 5), consistent with the findings in identified Ivy cells. The relatively low number of Ivy cells identified compared with the number of fast-spiking interneurons observed here might be explained by the spike sorting analysis, which favors the clustering of units with high discharge rate. This is also reflected by the strongly biased ratio of fast-spiking interneurons to pyramidal cells, which also fire at low discharge rates. Overall, our results show that slow-spiking interneurons in the CA1 pyramidal cell layer with characteristics similar to those of Ivy cells can be recognized in behaving animals.

Synaptic Transmission and Input-Output Organization of Ivy Cells

To study the intrinsic membrane properties of Ivy cells and their synaptic connections with neighboring CA1 pyramidal cells, dual intracellular recordings with sharp electrodes and biocytin-labeling were made in slices of adult rat hippocampus. Five Ivy cells were identified by their fine, dense axons, absence of large axonal varicosities, and short dendritic arbors (Figure 6A). The soma area in the largest cross-section (range, 109–262 μm^2) using the long (range, 13–23 μm) and short (range, 10–15 μm) axis, number of primary dendrites (five to seven), and density of axons as measured with axonal length (range, 2.0–3.5 mm) in defined areas as described for in vivo filled cells were measured in four of the recorded cells and are all comparable to the values obtained from Ivy cells recorded in vivo. The one putative Ivy cell tested was immunopositive for nNOS, and four Ivy cells tested were immunonegative for PV, supporting the axon-based classification (data not shown). Ivy cells exhibited delayed, stuttering, and adapting firing patterns (Figure 6B), similar to those of

other interneurons, but maximum firing rates were low and their action potentials much broader (width at half amplitude, 0.8 ± 0.2 ms) than those of fast-spiking cells such as bistratified cells (0.4 ± 0.1 ms, p = 0.005). These findings are consistent with extracellular recordings and provide another independent parameter for cell identification. Spike afterhyperpolarizations were similar in amplitude in the two cell types (Table 2), but six times broader in Ivy cells (width at half amplitude, 71.6 ± 38.8 ms) than in bistratified cells (12.3 ± 13.6 ms; p = 0.003).

Three of the five Ivy cells elicited inhibitory postsynaptic potentials (IPSPs) in simultaneously recorded pyramidal cells, and in four Ivy cells simultaneously recorded pyramidal cells elicited excitatory postsynaptic potentials (EPSPs), one pair being reciprocally connected. At excitatory connections from pyramidal cells, average EPSP amplitudes, failure rates, and short-term depression in Ivy (Figure 6D) and bistratified cells were similar, as were the average frequencies and amplitudes of spontaneous EPSPs (Table 2). The EPSPs elicited in Ivy cells, however, were significantly broader (width at half amplitude, 11.5 ± 1.5 ms) than those in bistratified cells (6.4 ± 2.7 ms; p = 0.016; Table 2) and O-LM cells (Ali and Thomson, 1998), though narrower than those elicited at pyramidal-pyramidal cell connections in CA1 (Deuchars and Thomson, 1996). Average IPSP amplitudes and widths at half amplitude were similar for Ivy and bistratified cell IPSPs (Table 2), but the rise times of IPSPs elicited by Ivy cells were significantly slower (12.5 ± 1.6 ms) than those of bistratified cell IPSPs (8.4 ± 3.2 ms; p = 0.014). No significant jitter in the onset latency of IPSPs, or any correlation between single-sweep IPSP amplitude and rise time, was observed (data not shown). Like many IPSPs recorded in mature pyramidal cells, the IPSPs elicited by Ivy cells exhibited short-term depression (Ali et al., 1998) (Figure 6E).

In order to investigate nNOS and NPY coexpressing cells located in CA1 stratum radiatum, we performed targeted whole-cell recordings (n = 46) and identified five Ivy cells with somata located in this layer (Figures S4 and S5). These cells had very dense axons mainly in stratum radiatum, and all five cells had radially extending dendrites in stratum radiatum. Four of these cells were tested for the expression of nNOS, and all four were found immunopositive; three out of three tested Ivy cells were immunopositive for NPY, and all five cells were immunonegative for the cannabinoid receptor CB1 (Figure S4, Table S5). Ivy cells in stratum radiatum generated broad action potentials with frequency adaptation. We compared the membrane responses of the five Ivy cells with those of CCK and CB1 coexpressing basket cells (n = 5), which constitute a well described cell class in this layer. The action potential half-width (1.04 ± 0.17 ms) and afterhyperpolarization half-width (33.6 ± 7.1 ms) of the five Ivy cells were significantly different (p = 0.008 and p = 0.016, respectively) from those of CCK-expressing basket cells (0.74 ± 0.09 ms; 59.4 ± 25.4 ms; additional measurements are stated in Table S5). In addition, we recorded unitary inhibitory postsynaptic currents (uIPSCs) in CA1 pyramidal cells evoked by Ivy cells with somata in stratum radiatum. Out of 21 attempts, we obtained 6 synaptically coupled interneuron-pyramidal cell pairs; two of the interneurons were identified as Ivy cells (Figure S5 and Table S5). The slow IPSCs evoked by the Ivy cells were small in amplitude (9.9 and 6.1 pA) and had a slow 10%–90% rise time (3.0 and 2.6 ms) and long half-width (17.8 and 15.8 ms) and decay time (13.6 and 18.5 ms). A comparison with faster uIPSCs evoked in CA1

pyramidal cells by CCK-expressing cells in stratum radiatum (n = 2) is shown in Table S5 and Figure S5.

DISCUSSION

Ivy Cells Constitute a Major and Distinct Neuronal Class in the Hippocampus

The knowledge of the powerful modulatory effects of NO and NPY on neuronal activity (Bacci et al., 2002; Burette et al., 2002; Colmers et al., 1987; Makara et al., 2007; Nugent et al., 2007) sharply contrasts with the little that is known about the identity of the large populations of nNOS- or NPY-expressing neurons (Allen et al., 1983; Czeh et al., 2005; Jinno and Kosaka, 2002). We have shown that interneurons coexpressing nNOS and NPY are more numerous in the CA1 pyramidal cell layer than any of the PV-expressing interneuron types, including the widely studied basket, axo-axonic, and bistratified cells (Ali et al., 1998; Buhl et al., 1994; Freund and Buzsaki, 1996; Fuchs et al., 2007; Jonas et al., 2004; Kawaguchi and Kondo, 2002; Pawelzik et al., 1999; Pawelzik et al., 2002). The spike timing during network oscillations, slow-firing characteristics, distinctive axonal arbors, and molecular constitution of these neurons led us to define a cell type, which we have named the Ivy cell. Although only a few Ivy cells could be labeled during electrophysiological recordings, the remarkable homogeneity of the multiple parameters measured in these cells, together with the immunofluorescence population survey, indicated a well-defined cell class. By detecting nNOS, NPY, and $GABA_AR$-α1, it was possible to recognize this cell type throughout the cerebral cortex.

Many Ivy cells were similar to bistratified cells in the position of their somata in the pyramidal cell layer and their axonal fields, distributed in some cases in both strata oriens and radiatum (Buhl et al., 1994; Klausberger et al., 2004; Pawelzik et al., 2002). However, our anatomical and physiological analysis shows two cell types making distinct contributions to hippocampal networks.

Another neuronal type, the neurogliaform cell, shares some features with Ivy cells, including dense axonal fields and slow synaptic transmission (Price et al., 2005; Szabadics et al., 2007). However, neurogliaform cells have only been reported in stratum lacunosum-moleculare and their dendritic and axonal arborizations overlap with the glutamatergic input from the entorhinal cortex (Price et al., 2005). The axonal field of Ivy cells, on the other hand, is aligned with the CA3 input to stratum oriens and radiatum. Axonal convergence with distinct glutamatergic inputs has been used as a key parameter for the definition of cell types (Somogyi et al., 1998). In addition, the short dendrites of neurogliaform cells are completely contained within their axonal clouds, whereas the dendrites of Ivy cells extend outside their axonal span. Because of their laminar location, the two cell types receive distinct glutamatergic and GABAergic inputs. Ivy cells can evoke repetitive inhibitory responses with short delays in pyramidal cells, in contrast to neurogliaform cells (Tamas et al., 2003). Importantly, neurogliaform and Ivy cells fire at different phases during hippocampal theta oscillations in vivo (P.F., T.K., and P.S., unpublished data), which demonstrates that the two cell classes contribute differentially to temporal computations, which we consider a key defining criterion to delineate cell types. Overall, neurogliaform and Ivy cells constitute distinct cell types, which might support similar contributions to the

Europe PMC Funders Author Manuscripts

network, but operate with distinct timing and at functionally distinct domains defined by separate glutamatergic inputs.

Ivy cells represent the most abundant interneuron type studied so far, but their identity has been overlooked. Physiologists may not have recognized them as interneurons because of their wide spikes, low firing rate, and location among the pyramidal cells; while anatomists, disregarding molecular expression profiles and spiking activity, may have mistaken the axons of Ivy cells for those of bistratified cells. In general, many studies have concentrated on the more easily recognizable, widely accepted interneuron classes, mainly comprising fast-spiking and PV-expressing cells.

Modulatory Effects of Ivy Cells

The broad spikes of Ivy cells might ensure reliable transmission of action potentials along the very thin axons, resulting in the release of GABA and probably NPY and NO; although action-potential-dependent, axonal release of the neuromodulators NO and NPY remains to be confirmed. Ivy cell axons made GABAergic synapses onto oblique and basal dendrites of pyramidal cells, evoking IPSPs with slower rise times than those of fast-spiking bistratified cells. Correlations between spike width and IPSP kinetics have also been reported for cortical interneurons (Ali et al., 2007). The IPSCs evoked by Ivy cells in CA1 pyramidal cells also appeared to have slower kinetics than those evoked by CCK-expressing basket cells. The differences in rise times of synaptic responses could depend on their distances from the recording site (Rall et al., 1967), but Ivy and bistratified cells target pyramidal dendritic shafts of similar diameter, and probably at similar distances from the soma. One explanation explored was whether there was variability in spike arrival time at the several synapses contributing to an IPSP, a variability or jitter that might result from the very fine axons, but single-sweep analysis provided no evidence for this suggestion. Whether the slow rise times result from $GABA_A$ receptors with slow kinetics, or from the time course of diffusion of GABA from distributed sites within the dense axonal cloud (Szabadics et al., 2007), remains to be determined.

The effect of NO in synaptic transmission has been studied mainly in relation to dendritic spines of pyramidal neurons, and its action on soluble guanylate-cyclase-expressing glutamatergic terminals (Burette et al., 2002). However, nNOS is also strongly expressed by Ivy cells, which may be a major source of NO (Czeh et al., 2005; Jinno and Kosaka, 2002). Although unstable, NO diffuses quickly and can maintain physiologically active concentrations at a considerable distance from its production site (Garthwaite and Boulton, 1995). This suggests that axons and dendrites of Ivy cells potentially affect nearby presynaptic and postsynaptic targets via NO release. Recently it has been shown that NO contributes to retrograde signaling in certain GABAergic synapses in the hippocampus (Makara et al., 2007; Szabadits et al., 2007); it can induce LTP in GABAergic synapses on dopaminergic neurons of the ventral tegmental area (Nugent et al., 2007) and potentiate GABA release in other systems (Li et al., 2002; Yu and Eldred, 2005). It will be interesting to investigate how NO released by Ivy cells modulates GABA release and synaptic activity in the hippocampal network.

Europe PMC Funders Author Manuscripts

Europe PMC Funders Author Manuscripts

Another line of evidence supports the hypothesis that Ivy cells are specialized in regulating presynaptic sites. The neuropeptide Y2 receptor is strongly expressed by Schaffer collateral/commissural fibers in the CA1 stratum radiatum and oriens (Stanic et al., 2006), and Ivy cells, with their dense axons in these layers, represent a major potential local source of NPY. Activation of Y2 receptors has been shown to mediate a decrease in glutamatergic transmission by selective inhibition of presynaptic N-type Ca^{2+} channels (Colmers et al., 1987). Therefore, Ivy cells may dynamically modulate glutamate release from the Schaffer collateral/commissural input. In addition, NPY may decrease pyramidal cell excitability by increasing GABA release from interneuron terminals (Bacci et al., 2002), and NPY and NO might contribute to neurovascular control (Hamel, 2006).

The Role of Ivy Cells in Network Activity

The fast synaptic transmission, high firing rates, and tight phase-coupling during network oscillations of PV-expressing interneurons endow them with optimal qualities for precisely controlling the timing of pyramidal cell activity (Csicsvari et al., 1999; Fuchs et al., 2007; Jonas et al., 2004; Klausberger et al., 2003; Pouille and Scanziani, 2001). The slower effects of GABA, NPY, and NO, on the other hand, indicate that Ivy cells might be better suited for downscaling presynaptic and postsynaptic excitability and supporting homeostasis in the network.

Ivy cells fired broad action potentials with frequency adaptation upon positive current injection in vitro and discharged at low frequencies during theta, gamma, and ripple oscillations in vivo; the in vivo firing patterns of Ivy cells located in stratum radiatum remains to be investigated. Intrinsic membrane properties, including long-lasting afterhyperpolarizations, which might shunt excitatory inputs for relatively long periods (~100 ms), might explain the slow-spiking character of Ivy cells. Due to the strongly depressing nature of their EPSPs, the relatively sparse spikes fired by Ivy cells during theta oscillations might be initiated by the concerted firing of a few presynaptic pyramidal cells that were previously silent. However, the lack of activation of Ivy cells during ripple oscillations indicates that these cells might be under strong inhibitory control, the source of which remains to be identified. The lack of firing in Ivy cells during most oscillatory cycles indicates that the maintenance of the rhythm and its exact timing is provided by fast-spiking and/or PV-expressing interneurons, which fire on most cycles (Csicsvari et al., 1999; Klausberger et al., 2003). The spiking activity of Ivy cells during some oscillatory cycles may inhibit a population of targeted pyramidal cell dendrites. The exact contribution of the highly abundant Ivy cells to hippocampal network function and their presynaptic or postsynaptic modulation of neuronal activity might be explored by future selective manipulation of the activity of this cell type.

EXPERIMENTAL PROCEDURES

All procedures involving experimental animals were carried out in accordance with the Animals (Scientific Procedures) Act, 1986 (UK) and associated procedures.

In Vivo Recording and Labeling

The four Ivy cells were obtained from four male Sprague-Dawley rats (250–350 g) anesthetized with urethane (1.25 g/kg of body weight) plus supplemental doses of ketamine and xylazine (20 and 2 mg/kg, respectively) as needed; body temperature was maintained with a heating pad. Neuronal activity in the hippocampus was recorded extracellularly with a glass electrode (15–25 MΩ) filled with 1.5% neurobiotin in 0.5 M NaCl, and the local field potential (LFP) was recorded with a nearby second electrode in CA1 stratum pyramidale. Single-unit activity (sampling rate, 20 kHz) and LFP (sampling rate, 1 kHz) were filtered online between 0.8–5 kHz and 0.3–300 Hz, respectively. Recorded cells were individually labeled with neurobiotin using the juxtacellular labeling method, only after data for the firing patterns had been sampled from the unaffected cell. Spike shape and amplitude were monitored during recording and labeling to ensure that the same cell was recorded and labeled. Two to four hours (P2a, 3 hr; T98e, 2 hr; T134a, 3.5 hr; T140b, 3 hr) after labeling, cardiac perfusion with saline was followed by ~20 min fixation with a fixative 4% paraformaldehyde, 15% v/v saturated picric acid, and 0.05% glutaraldehyde.

Recordings in nonanesthetized animals were performed in ten male rats (four Long Evans, two Hooded Lister, four Sprague-Dawley) with 4–16 independently movable wire tetrodes as described previously (Klausberger et al., 2005).

In Vitro Recording and Labeling

For sharp electrode recordings, male Wistar rats weighing between 140–200 g were anaesthetized in a halothane (ICI Pharmaceutics, UK) -saturated chamber, then given an intraperitoneal injection of sodium pentobarbitone (Euthatal, Vericore Ltd, Dundee, 60 mg/kg) and perfused transcardially with ice-cold modified artificial cerebrospinal fluid (ACSF) with added sodium pentobarbitone (60 mg/l), in which the NaCl was replaced with 248 mM sucrose. The rats were decapitated, the brain was removed, and 450-μm-thick coronal slices were cut (Vibroslice, Camden Instruments) and transferred to an interface recording chamber maintained at 34°C–35°C. The slices were maintained for 1 hr in sucrose containing ACSF; this was then replaced with standard ACSF in which all recordings were made, and which contained 124 mM NaCl, 25.5 mM $NaHCO_3$, 3.3 mM KCl, 1.2 mM KH_2PO_4, 1.0 mM $MgSO_4$, 2.5 mM $CaCl_2$, and 15 mM D-glucose, equilibrated with 95% O_2/5% CO_2 gas. Paired intracellular recordings were made using conventional sharp microelectrodes (resistances of 150–200 MΩ) containing 2 M potassium methylsulphate and 2% biocytin (w/v) under current-clamp conditions using an Axoprobe amplifier (Axon Instruments, Burlingame, CA). The cells were passively filled with biocytin while recording. After synaptically connected neurons were recorded, the slices were fixed, resectioned at 50 μm thickness, and histologically analyzed for identification of recorded neurons as described previously (Pawelzik et al., 1999).

For whole-cell recordings (33°C ± 1°C), male postnatal day 17–20 Sprague-Dawley rats were anaesthetized with isoflurane and decapitated, and acute slices of hippocampus were prepared as previously described (Price et al., 2005). Single and paired whole-cell recordings were performed using an EPC10/2 amplifier (HEKA, Lambrecht, Germany). The somata of the interneurons in the stratum radiatum of the CA1 area were visually identified

based on their shape and size. Borosilicate patch electrodes were filled with 126 mM K-gluconate, 10 mM HEPES, 10 mM Na_2Phosphocreatine, 4 mM KCl, 4 mM Mg-ATP, 0.3 mM Na_2-GTP, and 0.15% biocytin (pH 7.3) with KOH, and had resistances between 4 and 6 MΩ. Access resistance was always monitored to ensure the stability of recording conditions. In the paired recording experiments, putative presynaptic interneurons were voltage clamped at a holding potential of −60 mV, and the postsynaptic CA1 pyramidal neurons were held at −50 mV to enhance the driving force for the Cl^--mediated GABAergic responses. Action currents were elicited in one cell and the corresponding uIPSC was measured in the postsynaptic neuron. Histological analysis was performed as described previously (Price et al., 2005).

Tissue Processing and Anatomical Analysis of In Vivo Recorded Cells

Immunofluorescence and peroxidase reactions for light and electron microscopy and reconstruction of cells were performed with all necessary controls, as described previously (Klausberger et al., 2005). Neurons were reconstructed using a drawing tube; soma size and axonal length (by “skeletonizing” the axonal processes) were measured with ImageJ (NIH, Bethesda, MD). For immunofluorescence reactions, mixtures of up to four primary antibodies raised in different species were used; they are listed in Table S4. Secondary antibodies were conjugated to Alexa Fluor 488 (Invitrogen™, Molecular Probes™, Eugene, OR), AMCA™ (Jackson ImmunoResearch Laboratories, Inc., West Grove, PA), Cy™3 (idem), or Cy™5 (idem).

Electron microscopic analysis and target identification was performed as described previously (Klausberger et al., 2005). The 3D reconstruction from serial electron micrographs was performed using Reconstruct v1.0.3.0 (http://synapse-web.org/tools/index.stm, John C. Fiala) and Lightwave 3D® 8.5 (NewTek, Inc., San Antonio, TX).

The frequencies of coexpression of PV, NPY (rabbit antibody), and nNOS (mouse antibody) in interneurons were estimated in accordance with the optical disector principle. To cover the whole area of the CA1 region, three nonoverlapping scanning fields (field size: 750 × 750 μm) were delineated in each section. Stacks of 30–40 serial optical sections nominally 2 μm apart (referenced to the original 70 μm thickness of the Vibratome section to compensate for Z direction shrinkage) were recorded with a confocal laser-scanning microscope (CLSM; TCS-SP2; Leica Microsystems, Wetzlar, Germany) under a 20× objective lens (NA 0.75) for each field. Prior to the disector counting, we checked the penetration of each immunolabeling and found that antibodies to PV did not fully penetrate into the middle of 70-μm-thick sections, although those to NPY and nNOS penetrated completely. Because the height of unbiased counting space should be adjusted to the thickness of sections showing adequate immunostaining (Jinno and Kosaka, 2002), here we used the CLSM optical section at the physical cut surface as a look-up section, and those between 2 to 18 μm (referenced to the original 70 μm thickness of the Vibratome section) inside the surface as reference sections. The measuring and counting procedures were carried out by using an image-analysis software package, ImageJ 1.35 (NIMH, Bethesda, MD), with the Cell Counter plug-in (Kurt De Vos, University of Sheffield, Sheffield, UK).

Europe PMC Funders Author Manuscripts

Europe PMC Funders Author Manuscripts

The expression of $GABA_AR$-α1, CR, CB, SM, or α-actinin-2 in putative Ivy cells was assessed by epifluorescence microscopy in triple or quadruple immunoreactions by photographing (under a 40× objective lens, NA 0.7) nNOS-expressing cells in stratum pyramidale on both surfaces of the section in random, nonoverlapping fields.

Data Analysis for Recordings from Anaesthetized Rats

The detection of theta, non-theta/non-sharp wave and ripple episodes, the beginning, highest amplitude, and end of ripple episodes, and the calculation of discharge frequencies of single cells during different brain states, were achieved as described previously (Klausberger et al., 2003). Gamma oscillations were detected by digitally filtering (30–80 Hz) the LFP and selecting cycles with amplitude greater than the mean cycle amplitude computed over the entire duration of the recording; units and LFP were recorded from separate electrodes. To determine the firing phase histograms, the troughs of the oscillations were detected in the filtered LFP. Each spike was assigned to a given phase (bin size 18°) between the troughs (0° and 360°).

Seven bistratified cells (T79e, T83a, T89a, T92a, T96a, T104a, and T104b) published earlier (Baude et al., 2006; Klausberger et al., 2004) and two additional unpublished bistratified cells (C8b and P31a) were analyzed for comparison with Ivy cells.

Data Analysis for Recordings In Vivo in Drug-Free Rats

Unit isolation and clustering procedures have been described previously (Csicsvari et al., 1999). Data from some of these cells not related to the present study have been reported earlier (Klausberger et al., 2005; O'Neill et al., 2006), but here, new analysis was carried out. Putative fast-spiking cells (n = 86) were defined as units with spike durations shorter than 0.25 ms and first moment of their autocorrelogram being longer than 11 ms; pyramidal cells (n = 743) were defined as units with spike durations longer than 0.25 ms, the first moment of their autocorrelogram being shorter than 11 ms. Spike width was measured from the electrode with the highest spike amplitude after averaging action potentials, and was defined as the width of the waveform at 25% of the spike amplitude maximum relative to baseline.

Data Analysis for Recordings In Vitro

For sharp electrode recordings, data were digitized using an analog to digital converter (CED 1401, Cambridge, UK) at 10 kHz and filtered at 5 kHz (voltage resolution 0.005–0.01 mV) (Spike-2, Cambridge Electronic Designs, Cambridge, UK). Data were analyzed off-line using in-house software (developed by Dr. David West, School of Pharmacy, London, UK). Single sweeps were checked to ensure that every presynaptic action potential was recognized by the software and that the trigger points used for subsequent analysis were accurately aligned with the fast component of the rising phase of each action potential. Sweeps that included large artifacts that obscured the postsynaptic event were excluded. The amplitudes of EPSPs and IPSPs, 10%–90% rise times, and widths at half amplitudes were measured from averages of the first EPSPs or IPSPs (≥80 sweeps). Averages of second and third EPSPs and IPSPs were triggered from the rising phase of the second and third action potentials, respectively. Two of the cells included here as Ivy cells (970514HHP and

969711AHP) have been reported previously as bistratified cells (Ali et al., 1998; Pawelzik et al., 1999). In the light of our new data we reclassify them as Ivy cells. The physiological parameters of four bistratified cells (980513B, 970211A1, 960805A, and 960604B) used for comparison in this study have been reported previously (Ali et al., 1998; Pawelzik et al., 1999) and are included to provide a more comprehensive average; another eight bistratified cells are reported here for the first time.

For whole-cell recordings, data were analyzed off-line using Igor Pro 5.05 (Wavemetrics, Lake Oswego, OR). Failures were flagged if the uIPSCs were of smaller amplitude than three times the standard deviation (SD) of the baseline recording, had a time window smaller than 10 ms, or had an onset time that was greater than the average plus five times the SD calculated from files of 50 sweeps. The input resistance (R_{in}) was calculated from the slope of a line fitted to the subthreshold range on a plot of the injected current versus the steady-state membrane voltage when a family of hyperpolarizing and depolarzing current injections was applied. The decay time constant was calculated by fitting a single exponential to the response of the cell to a current injection of −30/−60 pA in current-clamp mode. The action potential half-width and afterhyperpolarization were measured from the initial point of the raising phase of the action potential. The peak amplitude, 10%–90% rise time, half-width, and decay time of the uIPSCs was analyzed from averages of 20–30 single uIPSCs.

Statistics

Unless stated, all tabulated data are presented as the mean ± SD, and exact Mann Whitney U-test was used for statistical comparisons between populations. Theta and gamma phases were analyzed using circular statistics. Significant differences were accepted at $p < 0.05$.

Supplementary Material

Refer to Web version on PubMed Central for supplementary material.

ACKNOWLEDGMENTS

We thank Kristina Detzner, Richard Hewer, Ben Micklem, David Roberts, and Wai Yee Suen for excellent technical assistance; Icnelia Huerto-Ocampo for histological, immunofluorescence, and ultra structural analysis; Viktor Szigeti for the reconstruction and anatomical analysis of cell P2 presented in Figure 2; Jojanneke Huck for supervision in electron microscopy; Yannis Dalezios for help with statistics; and Gyorgy Buzsaki, Dimitri Kullmann, and Karri Lamsa for comments on an earlier version of the manuscript. We thank the following scientists for their generous gift of antibodies (to molecule): K.G. Baimbridge (PV), A. Beggs (α-actinin-2), A. Buchan (SM), T. Gorcs (VIP), T. Kaneko (PPTA and PPTB), E. Mugnaini (GAD), G. Ohning (VIP), R. Shigemoto (mGluR8a), W. Sieghart ($GABA_A$R-α1), A. Varro (pro-CCK), and M. Watanabe (mGluR1α). This work was supported by a STREP grant, INTERDEVO (LSHM-CT-2004-005139) in the Framework 6 program of the European Union. T.K. was also supported by grant P16637-B02 of the Austrian Science Fund. R.B. was supported by a studentship funded by Novartis Pharma and GSK and by the Medical Research Council.

REFERENCES

Ali AB, Thomson AM. Facilitating pyramid to horizontal oriensalveus interneurone inputs: dual intracellular recordings in slices of rat hippocampus. J. Physiol. 1998; 507:185–199. [PubMed: 9490837]

Ali AB, Deuchars J, Pawelzik H, Thomson AM. CA1 pyramidal to basket and bistratified cell EPSPs: dual intracellular recordings in rat hippocampal slices. J. Physiol. 1998; 507:201–217. [PubMed: 9490840]

Ali AB, Bannister AP, Thomson AM. Robust correlations between action potential duration and the properties of synaptic connections in layer 4 interneurones in neocortical slices from juvenile rats and adult rat and cat. J. Physiol. 2007; 580:149–169. [PubMed: 17234697]

Allen YS, Adrian TE, Allen JM, Tatemoto K, Crow TJ, Bloom SR, Polak JM. Neuropeptide Y distribution in the rat brain. Science. 1983; 221:877–879. [PubMed: 6136091]

Arancio O, Kiebler M, Lee CJ, Lev-Ram V, Tsien RY, Kandel ER, Hawkins RD. Nitric oxide acts directly in the presynaptic neuron to produce long-term potentiation in cultured hippocampal neurons. Cell. 1996; 87:1025–1035. [PubMed: 8978607]

Bacci A, Huguenard JR, Prince DA. Differential modulation of synaptic transmission by neuropeptide Y in rat neocortical neurons. Proc. Natl. Acad. Sci. USA. 2002; 99:17125–17130. [PubMed: 12482942]

Baude A, Bleasdale C, Dalezios Y, Somogyi P, Klausberger T. Immunoreactivity for the $GABA_A$ receptor α1 subunit, somatostatin and connexin 36 distinguishes axo-axonic, basket and bistratified interneurons of the rat hippocampal. Cereb. Cortex. 2006; 17:2094–2107. [PubMed: 17122364]

Buhl EH, Halasy K, Somogyi P. Diverse sources of hippocampal unitary inhibitory postsynaptic potentials and the number of synaptic release sites. Nature. 1994; 368:823–828. [PubMed: 8159242]

Burette A, Zabel U, Weinberg RJ, Schmidt H, Valtschanoff JG. Synaptic localization of nitric oxide synthase and soluble guanylyl cyclase in the hippocampus. J. Neurosci. 2002; 22:8961–8970. [PubMed: 12388603]

Buzsaki G, Leung L-W, Vanderwolf CH. Cellular bases of hippocampal EEG in the behaving rat. Brain Res. 1983; 287:139–171. [PubMed: 6357356]

Colmers WF, Lukowiak K, Pittman QJ. Presynaptic action of neuropeptide Y in area CA1 of the rat hippocampal slice. J. Physiol. 1987; 383:285–299. [PubMed: 2821236]

Connors BW, Gutnick MJ, Prince DA. Electrophysiological properties of neocritical neurons in vitro. J. Neurophysiol. 1982; 48:1302–1320. [PubMed: 6296328]

Csicsvari J, Hirase H, Czurko A, Mamiya A, Buzsaki G. Oscillatory coupling of hippocampal pyramidal cells and interneurons in the behaving rat. J. Neurosci. 1999; 19:274–287. [PubMed: 9870957]

Csicsvari J, Jamieson B, Wise KD, Buzsaki G. Mechanisms of gamma oscillations in the hippocampus of the behaving rat. Neuron. 2003; 37:311–322. [PubMed: 12546825]

Czeh B, Hajnal A, Seress L. NADPH-diaphorase positive neurons of the rat hippocampal formation: regional distribution, total number and colocalization with calcium binding proteins. Prague Med. Rep. 2005; 106:261–274.

Deuchars J, Thomson AM. CA1 pyramid-pyramid connections in rat hippocampus in vitro: dual intracellular recordings with biocytin filling. Neuroscience. 1996; 74:1009–1018. [PubMed: 8895869]

Foster DJ, Wilson MA. Reverse replay of behavioural sequences in hippocampal place cells during the awake state. Nature. 2006; 440:680–683. [PubMed: 16474382]

Freund TF, Buzsaki G. Interneurons of the hippocampus. Hippocampus. 1996; 6:347–470. [PubMed: 8915675]

Fuchs EC, Zivkovic AR, Cunningham MO, Middleton S, Lebeau FE, Bannerman DM, Rozov A, Whittington MA, Traub RD, Rawlins JN, Monyer H. Recruitment of parvalbumin-positive interneurons determines hippocampal function and associated behavior. Neuron. 2007; 53:591–604. [PubMed: 17296559]

Garthwaite J, Boulton CL. Nitric oxide signaling in the central nervous system. Annu. Rev. Physiol. 1995; 57:683–706. [PubMed: 7539993]

Hamel E. Perivascular nerves and the regulation of cerebrovascular tone. J. Appl. Physiol. 2006; 100:1059–1064. [PubMed: 16467392]

Jinno S, Kosaka T. Patterns of expression of calcium binding proteins and neuronal nitric oxide synthase in different populations of hippocampal GABAergic neurons in mice. J. Comp. Neurol. 2002; 449:1–25. [PubMed: 12115690]

Jonas P, Bischofberger J, Fricker D, Miles R. Interneuron Diversity series: Fast in, fast out – temporal and spatial signal processing in hippocampal interneurons. Trends Neurosci. 2004; 27:30–40. [PubMed: 14698608]

Kawaguchi Y, Kondo S. Parvalbumin, somatostatin and cholecystokinin as chemical markers for specific GABAergic interneuron types in the rat frontal cortex. J. Neurocytol. 2002; 31:277–287. [PubMed: 12815247]

Klausberger T, Magill PJ, Marton L, Roberts JDB, Cobden PM, Buzsáki G, Somogyi P. Brain state- and cell type-specific firing of hippocampal interneurons in vivo. Nature. 2003; 421:844–848. [PubMed: 12594513]

Klausberger T, Marton LF, Baude A, Roberts JDB, Magill P, Somogyi P. Spike timing of dendrite-targeting bistratified cells during hippocampal network oscillations in vivo. Nat. Neurosci. 2004; 7:41–47. [PubMed: 14634650]

Klausberger T, Marton LF, O'Neill J, Huck JHJ, Dalezios Y, Fuentealba P, Suen WY, Papp E, Kaneko T, Watanabe M, et al. Complementary roles of cholecystokinin- and parvalbumin- expressing GABAergic neurons in hippocampal network oscillations. J. Neurosci. 2005; 25:9782–9793. [PubMed: 16237182]

Li DP, Chen SR, Pan HL. Nitric oxide inhibits spinally projecting paraventricular neurons through potentiation of presynaptic GABA release. J. Neurophysiol. 2002; 88:2664–2674. [PubMed: 12424302]

Makara JK, Katona I, Nyiri G, Nemeth B, Ledent C, Watanabe M, de Vente J, Freund TF, Hajos N. Involvement of nitric oxide in depolarization-induced suppression of inhibition in hippocampal pyramidal cells during activation of cholinergic receptors. J. Neurosci. 2007; 27:10211–10222. [PubMed: 17881527]

Martina M, Schultz JH, Ehmke H, Monyer H, Jonas P. Functional and molecular differences between voltage-gated K+ channels of fast-spiking interneurons and pyramidal neurons of rat hippocampus. J. Neurosci. 1998; 18:8111–8125. [PubMed: 9763458]

McCormick DA, Connors BW, Lightall JW, Prince DA. Comparative electrophysiology of pyramidal and sparsely spiny stellate neurons of the neocortex. J. Neurophysiol. 1985; 54:782–806. [PubMed: 2999347]

Miles R, Toth K, Gulyas AI, Hajos N, Freund TF. Differences between somatic and dendritic inhibition in the hippocampus. Neuron. 1996; 16:815–823. [PubMed: 8607999]

Nitz D, McNaughton B. Differential modulation of CA1 and dentate gyrus interneurons during exploration of novel environments. J. Neurophysiol. 2004; 91:863–872. [PubMed: 14523073]

Nugent FS, Penick EC, Kauer JA. Opioids block long-term potentiation of inhibitory synapses. Nature. 2007; 446:1086–1090. [PubMed: 17460674]

O'Keefe, J.; Nadel, L. The Hippocampus as a Cognitive Map. Clarendon; Oxford: 1978.

O'Neill J, Senior T, Csicsvari J. Place-selective firing of CA1 pyramidal cells during sharp wave/ripple network patterns in exploratory behavior. Neuron. 2006; 49:143–155. [PubMed: 16387646]

Pawelzik H, Bannister AP, Deuchars J, Ilia M, Thomson AM. Modulation of bistratified cell IPSPs and basket cell IPSPs by pentobarbitone sodium, diazepam and Zn^{2+}: dual recordings in slices of adult rat hippocampus. Eur. J. Neurosci. 1999; 11:3552–3564. [PubMed: 10564363]

Pawelzik H, Hughes DI, Thomson AM. Physiological and morphological diversity of immunocytochemically defined parvalbumin- and cholecystokinin-positive interneurones in CA1 of the adult rat hippocampus. J. Comp. Neurol. 2002; 443:346–367. [PubMed: 11807843]

Pouille F, Scanziani M. Enforcement of temporal fidelity in pyramidal cells by somatic feed-forward inhibition. Science. 2001; 293:1159–1163. [PubMed: 11498596]

Price CJ, Cauli B, Kovacs ER, Kulik A, Lambolez B, Shigemoto R, Capogna M. Neurogliaform neurons form a novel inhibitory network in the hippocampal CA1 area. J. Neurosci. 2005; 25:6775–6786. [PubMed: 16033887]

Rall W, Burke RE, Smith TG, Nelson PG, Frank K. Dendritic location of synapses and possible mechanisms for the monosynaptic EPSP in motoneurons. J. Neurophysiol. 1967; 30:1169–1193. [PubMed: 4293410]

Ranck JB Jr. Studies on single neurons in dorsal hippocampal formation and septum in unrestrained rats. Part 1. Behavioral correlates and firing repertoires. Exp. Neurol. 1973; 42:461–531. [PubMed: 4355646]

Rudy B, McBain CJ. Kv3 channels: voltage-gated K+ channels designed for high-frequency repetitive firing. Trends Neurosci. 2001; 24:517–526. [PubMed: 11506885]

Schwartzkroin PA, Kunkel DD. Morphology of identified interneurons in the CA1 regions of guinea pig hippocampus. J. Comp. Neurol. 1985; 232:205–218. [PubMed: 2982925]

Singer W, Gray CM. Visual feature integration and the temporal correlation hypothesis. Annu. Rev. Neurosci. 1995; 18:555–586. [PubMed: 7605074]

Soltesz I, Deschenes M. Low- and high-frequency membrane potential oscillations during theta activity in CA1 and CA3 pyramidal neurons of the rat hippocampus under ketamine-xylazine anesthesia. J. Neurophysiol. 1993; 70:97–116. [PubMed: 8395591]

Somogyi P, Klausberger T. Defined types of cortical interneurone structure space and spike timing in the hippocampus. J. Physiol. 2005; 562:9–26. [PubMed: 15539390]

Somogyi P, Tamas G, Lujan R, Buhl EH. Salient features of synaptic organisation in the cerebral cortex. Brain Res. Brain Res. Rev. 1998; 26:113–135. [PubMed: 9651498]

Stanic D, Brumovsky P, Fetissov S, Shuster S, Herzog H, Hokfelt T. Characterization of neuropeptide Y2 receptor protein expression in the mouse brain. I. Distribution in cell bodies and nerve terminals. J. Comp. Neurol. 2006; 499:357–390. [PubMed: 16998904]

Steriade M, Timofeev I, Grenier F. Natural waking and sleep states: a view from inside neocortical neurons. J. Neurophysiol. 2001; 85:1969–1985. [PubMed: 11353014]

Szabadics J, Tamas G, Soltesz I. Different transmitter transients underlie presynaptic cell type specificity of GABAA,slow and GABAA,fast. Proc. Natl. Acad. Sci. USA. 2007; 104:14831–14836. [PubMed: 17785408]

Szabadits E, Cserep C, Ludanyi A, Katona I, Gracia-Llanes J, Freund TF, Nyiri G. Hippocampal GABAergic synapses possess the molecular machinery for retrograde nitric oxide signaling. J. Neurosci. 2007; 27:8101–8111. [PubMed: 17652601]

Tamas G, Lörincz A, Simon A, Szabadics S. Identified sources and targets of slow inhibition in the neocortex. Science. 2003; 299:1902–1905. [PubMed: 12649485]

Toledo-Rodriguez M, Blumenfeld B, Wu C, Luo J, Attali B, Goodman P, Markram H. Correlation maps allow neuronal electrical properties to be predicted from single-cell gene expression profiles in rat neocortex. Cereb. Cortex. 2004; 14:1310–1327. [PubMed: 15192011]

Vanderwolf CH. Hippocampal electrical activity and voluntary movement in the rat. Electroencephalogr. Clin. Neurophysiol. 1969; 26:407–418. [PubMed: 4183562]

Yu D, Eldred WD. Nitric oxide stimulates gamma-aminobutyric acid release and inhibits glycine release in retina. J. Comp. Neurol. 2005; 483:278–291. [PubMed: 15682393]

Europe PMC Funders Author Manuscripts

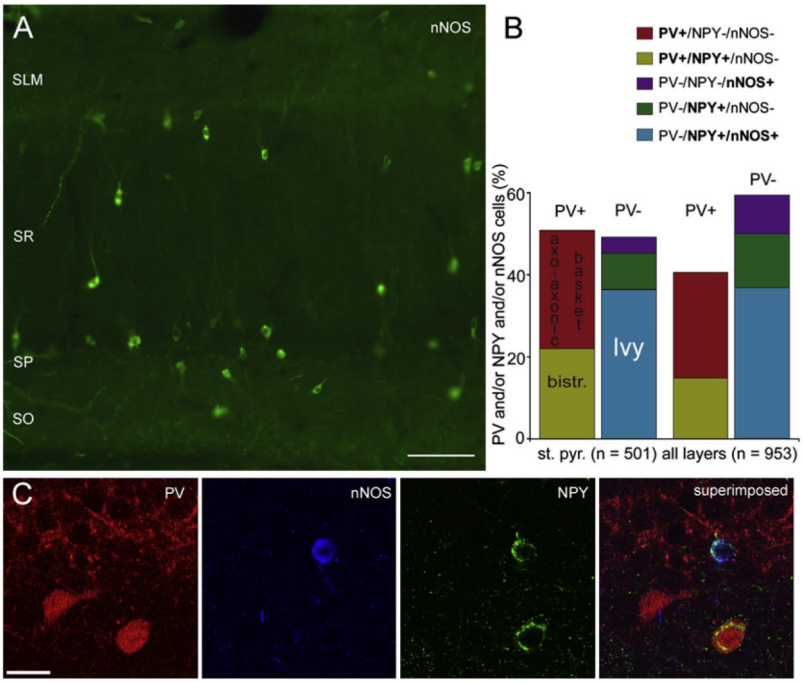

Figure 1. Abundance of nNOS- and NPY-Expressing Interneurons in the Hippocampus

(A) Epifluorescence micrograph illustrating the abundance of neuronal nitric oxide synthase (nNOS) immnunolabeled cells in the dorsal CA1 area. Most cells are located in and around stratum pyramidale.

(B) Unbiased quantification of interneurons immunoreactive for PV or nNOS and/or NPY in coronal sections of stratum pyramidale (st. pyr.) and the entire dorsal CA1 area (all layers). PV-expressing cells in the stratum pyramidale include basket and axo-axonic cells, which are negative for NPY, and bistratified cells, which are positive for NPY. Note that nNOS and NPY double-positive cells constitute the largest group.

(C) Confocal fluorescence micrographs showing immunolabeling for PV, nNOS, and NPY at the border of strata pyramidale and oriens.

Scale bars: (A), 100 μm; (C), 20 μm.

Europe PMC Funders Author Manuscripts

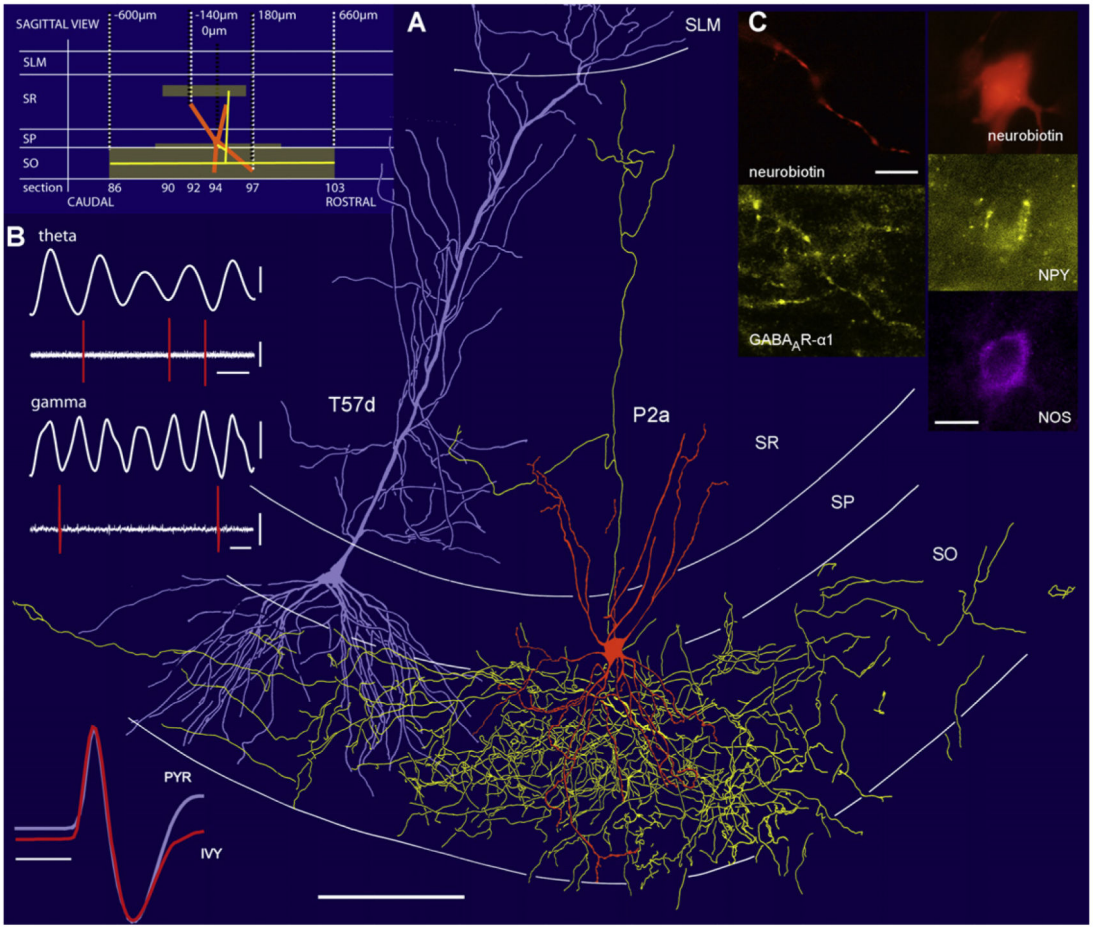

Figure 2. Firing Patterns, Molecular Characteristics, and Spatial Distribution of an Ivy Cell Recorded In Vivo

(A) Schematic sagittal view (top left) of the axonal (yellow) and dendritic (orange) fields and reconstruction in the coronal plane of a neurobiotin-labeled Ivy cell (P2a). The soma and dendrites are shown from all sections; the axon is presented only from three 70-µm-thick sections for clarity. Note the very dense axon in stratum oriens. A pyramidal cell (T57d, blue) recorded in another animal is added for illustrating spatial relationships. (Bottom left) Scaled, superimposed extracellular action potential waveform averages from the Ivy cell (orange) and pyramidal cell (blue) with similar shape and time course.

(B) The Ivy cell discharged sparsely but phase locked to the trough of the extracellularly recorded theta (filtered 3–6 Hz, top) and gamma (filtered 30–80 Hz, bottom) oscillations in stratum pyramidale.

(C) Fluorescence micrographs showing immunoreactivity for nNOS and NPY in the soma, and for the α1 subunit of the $GABA_A$ receptor in a dendrite.

Scale bars: (A), 100 µm, 1 ms; (B), filtered 0.2 mV, units, 0.5 mV; theta, 200 ms; gamma, 20 ms; (C), 10 µm.

Europe PMC Funders Author Manuscripts

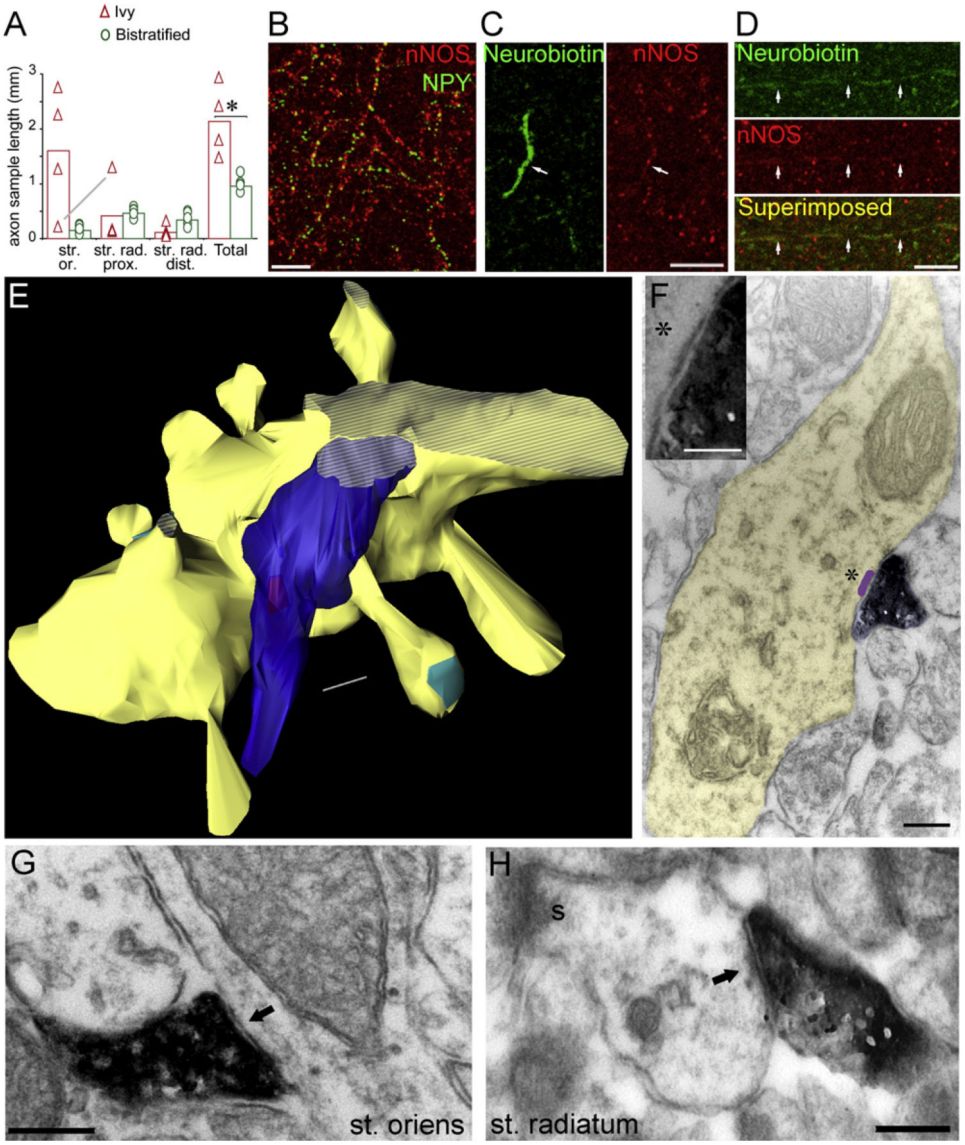

Figure 3. Axonal Arborizations and Synaptic Targets of Ivy Cells

(A) Axonal distributions of Ivy cells (n = 4) and bistratified cells (n = 5) are significantly different (*p = 0.016). Axons were sampled in defined areas (see text) of stratum oriens (str. or.), proximal stratum radiatum (str. rad. prox.), and next to stratum lacunosum-moleculare in distal stratum radiatum (str. rad. dist.) from one 70-μm-thick section containing the soma. Bars represent means, and symbols, individual measurements. The axonal sample of Ivy cells in stratum oriens was one order of magnitude higher than that of bistratified cells (1.604 ± 0.564 and 0.148 ± 0.033 mm, respectively). The Ivy cell (T134a) with the lowest amount of axon in stratum oriens had the highest amount in stratum radiatum (gray line). (B) Confocal immunoflourescence image showing a dense cloud of nNOS- and NPY-expressing, fine axons in stratum oriens. (C and D) Confocal immunoflourescence images showing the filled axon of Ivy cell P2a, which is immunopositive for nNOS. (E) Serial section reconstruction (12 70-nm-thick sections) of the Ivy cell bouton (blue) shown in (F)

making a synapse (purple) onto a small dendritic shaft (yellow) emitting multiple spines, some of them with visible type I synapses on their head (turquoise) appearing in this orientation. Dashed regions indicate cut surfaces. Inset in (F) shows the synaptic cleft and the small synaptic junction. (G and H) Electron micrographs of horseradish peroxidase product-labeled boutons of recorded Ivy cells. The boutons make small type II synaptic junctions (arrow) with small dendritic shafts either in stratum oriens ([G], cell P2a) or in stratum radiatum ([H], cell T134a). The small pyramidal cell dendrite in (H) emits a spine that receives a type I synapse. Scale bars: (B)–(D), 5 μm; (E)–(H), 200 nm; (F) inset, 100 nm.

Europe PMC Funders Author Manuscripts

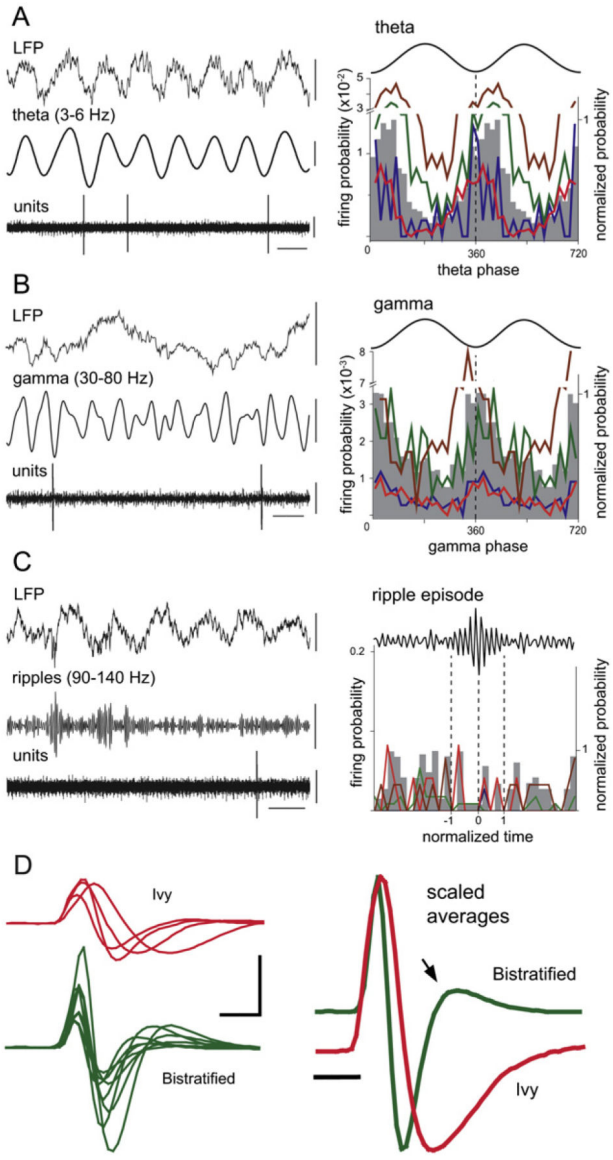

Figure 4. Firing Patterns of Identified Ivy Cells during Spontaneous Oscillations in Anaesthetized Rats

(A–C) (Left) Examples of the local field potential (LFP) filtered 0.3–300 Hz, or filtered for (A) theta oscillations (3–6 Hz), (B) gamma oscillations (30–80 Hz), or (C) sharp wave-associated ripples (90–140 Hz). (Left bottom) Single-unit activity (filtered 0.8–5 kHz) from an identified Ivy cell (T134a). The cell fired sparsely around the trough of the theta and gamma cycles. (Right) Phase histograms for four Ivy cells (colored traces) during (A) theta, (B) gamma, and (C) ripple oscillations; the normalized average phase distribution is shown in gray. For clarity, the same data are repeated in two cycles. The troughs of the extracellularly recorded oscillations are at 0°, 360°, and 720°; bin size is 18°. During ripple episodes (normalized times) the average firing probability of Ivy cells did not change relative to prerippple and postripple periods. The onset, highest amplitude, and end of normalized ripple episodes are marked as −1, 0, and 1, respectively (dotted lines).

(D) (Left) Average extracellular action potential waveforms of identified Ivy cells (red, n = 4) and bistratified cells (green, n = 8). (Right) Spike waveform grand averages from Ivy cells (red) and bistratified cells (green) peak-scaled for time course comparison. The difference in duration was statistically significant (see text for details). Arrow: the repolarizing phase of bistratified cell action potentials occurs much faster than that of Ivy cells.

Vertical scale bars: LFP, 0.5 mV; theta, 0.2 mV; gamma and ripples, 0.1 mV; units, 0.5 mV; and waveforms, 1 mV. Horizontal scale bars: (A) and (C), 200 ms; (B), 20 ms; (D), 0.5 ms.

Europe PMC Funders Author Manuscripts

Europe PMC Funders Author Manuscripts

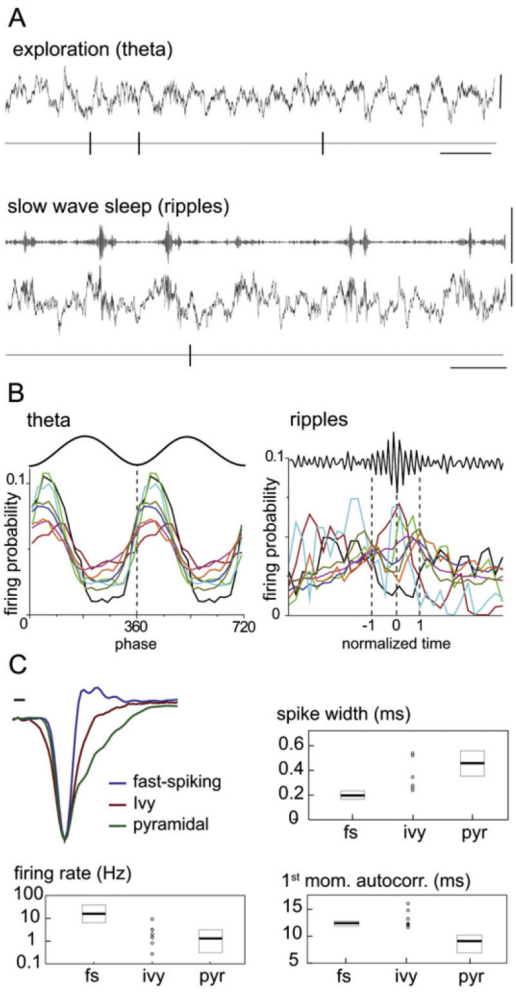

Figure 5. Firing Patterns of Interneurons Resembling Ivy Cells in Behaving Rats

(A) Spike train of an interneuron during theta oscillations in exploration, and relative to ripple oscillation in slow-wave sleep recorded by tetrodes implanted in the CA1 stratum pyramidale. Note the low firing rate and phase preferences during both rhythms, similar to identified Ivy cells.

(B) Firing probability distribution of eight putative interneurons during theta and ripple oscillations resembling the patterns seen in identified Ivy cells.

(C) Average extracellular action potential waveforms of putative fast-spiking (n = 86), Ivy (n = 8), and pyramidal (n = 743) cell populations. Fast-spiking cells were defined by a spike duration of <0.25 ms. Panels show spike width, firing rate, and the first moment of the autocorrelation for the same fast-spiking (fs), Ivy, and pyramidal (pyr) cells. Note that putative Ivy cells discharge at low frequencies, similar to pyramidal cells, but unlike the latter Ivy cells do not fire complex spike bursts as indicated by the first moment of the autocorrelation. Circles indicate individual putative Ivy cells. Medians and interquartile ranges are shown for each parameter by horizontal bars and boxes, respectively.

Scale bars: (A) ripples and theta, 0.3 mV; theta, 300 ms; ripples, 500 ms; (C), 0.1 ms.

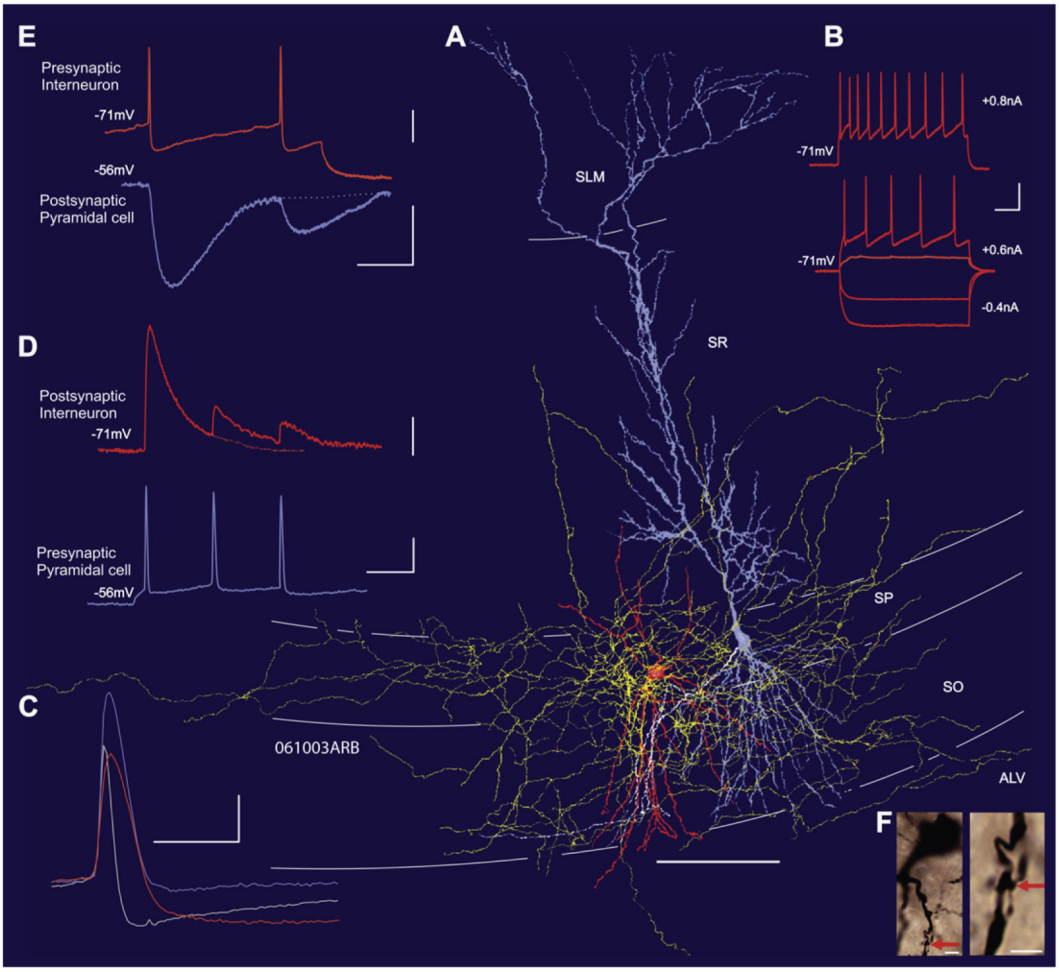

Figure 6. Synaptic Transmission and Reconstruction of a Reciprocally Connected Ivy and Pyramidal Cell Pair in the CA1 Region of the Hippocampus

(A) Reconstruction (from a 450-μm-thick slice) of the Ivy cell (soma/dendrites in orange, axon in yellow) and the pyramidal cell (soma/dendrites in light blue, axon in white). A large portion of the interneuron's axonal arbor is located in stratum pyramidale and stratum oriens, with very few collaterals extending into stratum radiatum and alveus.

(B) Responses of the Ivy cell to injected current pulses, demonstrating the frequency adaptation seen in these interneurons.

(C) Action potentials elicited by just suprathreshold current pulses in the pyramidal cell (mauve trace), the Ivy cell (orange trace), and a bistratified cell recorded in another experiment (gray trace) are superimposed. The Ivy cell action potential is similar in width to that of the pyramidal cell and is considerably broader than the action potential in the bistratified cell.

(D) Composite averages of the excitatory postsynaptic potentials (EPSPs) elicited by the pyramidal cell in the Ivy cell, demonstrating the strong paired pulse and brief train depression typical of these inputs.

(E) Composite averages of the inhibitory postsynaptic potentials (IPSPs) elicited by the Ivy cell in the pyramidal cell, demonstrating the typically slow time course and paired pulse depression of the IPSPs.

(F) Photomicrographs of the Ivy cell at two different magnifications to illustrate a putative synaptic input from the pyramidal cell to the interneuron (red arrows). Two such putative contacts were identified. The lower bouton and contact site is directly above the dendrite and not visible on this micrograph.

Vertical scale bars: (B), 20 mV; (C), 20 mV; (D) EPSPs, 2 mV; spike, 20 mV; (E) spike, 20 mV; IPSP, 1 mV. Horizontal scale bars: (A), 100 μm; (B), 40 ms; (C), 2 ms; (D), 20 ms; (E), 50 ms; (F) left, 5 μm; right, 2.5 μm.

Europe PMC Funders Author Manuscripts

Table 1
Molecular Expression Profile of Ivy Cells as Tested by Immunocytochemistry

Cell	P2a	T98e	T134a	T140b
nNOS	+	+	+	+
NPY	+	nt	+	+
$GABA_AR$ α1	+	nt	+	+
GAD	+	+	nt	+
PV	−	−	−	−
SM	−	−	−	−
CCK	−	nt	−	−
CB	−	−	−	nt
VIP	nt	−	−	−
CR	−	nt	−	nt
Kv3.1b	−	nt	nt	−
M2 receptor	−	−	nt	nt
PPTA	−	nt	−	nt
PPTB	nt	nt	−	−
mGluR1α	−	nt	nt	nt
mGluR8α	nt	−	nt	nt
α-actinin-2	−	nt	nt	nt
μ-opioid receptor	−	nt	nt	nt

M2, muscarinic receptor 2; nt, not tested; PPTA, pre-protachikinin-A; PPTB, pre-protachikinin-B.

Table 2

Comparison of the Electrophysiological Characteristics of Ivy and Bistratified Cells and the Properties of Their Synaptic Connections with Pyramidal Cells Recorded Intracellularly In Vitro

Interneuron type	Action Potential			Input resistance (MΩ)	Time constant (ms)
	Half-width (ms)	AHP amplitude (mV)	AHP half-width (ms)		
Ivy (n = 5)	0.8 ± 0.2*	13.6 ± 3.8	71.6 ± 38.8*	72.8 ± 53.6	7.6 ±4.1
Bistratified (n = 10)	0.4 ± 0.1	13.4 ± 3.8	12.3 ± 13.6	52.9 ± 21.1	5.9 ± 1.8

Presynaptic interneuron	Evoked IPSPs				Postsynaptic membrane potential (mV)
	Amplitude (mV)	10%-90% rise time (ms)	Half-width (ms)	Failure rate (%)	
Ivy (n = 4)	0.8 ± 0.4	12.5 ± 1.6*	54.1 ± 13.8	11.6 ± 8.0	−57 ±2.6
Bistratified (n = 8)	0.8 ± 0.6	8.4 ± 3.2	42.1 ± 17.0	7.8 ± 4.3	−53 ± 5.1

Postynaptic interneuron	Spontaneous EPSPs		Evoked EPSPs					Membrane potential (mV)
	Rate (Hz)	Amplitude (mV)	Amplitude (mV)	10%-90% rise time (ms)	Half-width (ms)	Failure rate (%)	$2^{nd}/1^{st}$ EPSP (%)	
Ivy (n = 5)	11.5 ± 3.7	2.7 ± 1.2	2.9 ± 2.2	1.5 ± 0.3	11.5 ± 1.5*	2.1 ± 2.3	39 ± 7.5	−65.8 ± 5.4
Bistratified (n = 4)	18.1 ± 5.5	1.1 ± 0.3	1.8 ± 2.3	1.5 ± 0.3	6.4 ± 2.7	1.4 ± 2.5	27.6 ± 7.1	−69.5 ± 5.7

AHP, afterhyperpolarization.

* $p < 0.05$.